Energy & Environmental Science

ROYAL SOCIETY OF CHEMISTRY

MINIREVIEW

View Article Online
View Journal | View Issue

Cite this: *Energy Environ. Sci.*, 2025, **18**, 6530

Solid-state electrolytes expediting interface-compatible dual-conductive cathodes for all-solid-state batteries

Shumin Zhang,[a] Feipeng Zhao,[c] Liang Li*[a] and Xueliang Sun *[b]

Received 30th March 2025,
Accepted 12th May 2025

DOI: 10.1039/d5ee01767j

rsc.li/ees

With the rapid development of solid-state electrolytes (SSEs), high-performance cathode materials specifically designed for all-solid-state batteries (ASSBs) are attracting increasing attention. Achieving interfacial compatibility between the continuously advancing SSEs and cathode active materials (CAMs) is crucial for the realization of advanced ASSBs. Recently, the emergence of interface-compatible dual-conductive (ICDC) cathodes has opened up a novel pathway towards developing ASSBs with high energy density and cost efficiency. ICDC cathodes refer to single cathode materials engineered to simultaneously achieve mixed ionic–electronic conductivity while ensuring good compatibility with SSEs in ASSBs. This innovative research topic has been propelled by the ongoing evolution of SSEs. In this minireview, we first discuss the progress in the mutual enhancement of SSEs and cathode materials, with a focus on addressing interface compatibility and dual conductivity challenges faced by conventional layered oxide CAMs in advanced sulfide- or halide-based ASSBs. Then, we outline two primary approaches for achieving ICDC cathodes: sulfurization and halogenation. Finally, we present an outlook, highlighting unresolved questions and future research directions. This minireview provides not only a summary of advancements in ICDC cathodes, but also fundamental guidance to inspire further exploration of cathode materials to be integrated with the state-of-the-art SSEs.

Broader context

The advancement of solid-state electrolytes (SSEs) has brought increasing attention to high-performance cathode materials that are specifically tailored for all-solid-state lithium batteries (ASSLBs). Ensuring compatibility between these evolving SSEs and cathode materials is critical for the development of efficient ASSLBs. Recently, interface-compatible dual-conductive (ICDC) cathodes, which exhibit both mixed ionic–electronic conductivity and interfacial compatibility with SSEs within a single material, have garnered increasing attention. These cathodes offer a promising pathway toward ASSLBs with both high energy density and cost efficiency. This minireview begins by exploring the mutual advancements in SSEs and cathode materials aimed at achieving interfacial compatibility and improved ionic/electronic conductivity when applying conventional layered oxide cathodes in the latest sulfide- or halide-based ASSLBs. It then outlines two key strategies—sulfurization and halogenation—that enable the realization of single cathode materials compatible with homo-category SSEs and the dual-conduction capability (Li-ion and electron) simutaniously. Finally, we provide an outlook in this field, highlighting unresolved challenges and identifying future research directions. This minireview aims to summarize recent progress in ICDC cathode materials while offering guidance for the development of next-generation cathode materials in synergy with advanced SSEs.

1. Introduction

All-solid-state lithium batteries (ASSLBs) are promising energy storage devices with high safety and energy density, due to the use of non-flammable inorganic solid-state electrolytes (SSEs) matching with Li metal anodes and conventional layered oxide cathode active materials (CAMs).[1,2] Given the relatively fixed selection of electrode materials which have been well established in traditional lithium-ion batteries (LIBs) using liquid electrolytes, numerous studies have focused on developing desirable SSEs for integration with existing electrode materials

[a] *School of Physical Science and Technology, Jiangsu Key Laboratory of Frontier Material Physics and Devices, Suzhou Key Laboratory of Intelligent Photoelectric Perception, Jiangsu Key Laboratory of Advanced Negative Carbon Technologies, Center for Energy Conversion Materials & Physics (CECMP), Soochow University, Suzhou, 215006, P. R. China. E-mail: lli@suda.edu.cn*
[b] *Ningbo Key Laboratory of All-Solid-State Battery, Eastern Institute for Advanced Study, Eastern Institute of Technology, Ningbo, P. R. China. E-mail: xsun@eitech.edu.cn*
[c] *Institute of Functional Nano & Soft Materials (FUNSOM), Soochow University, Suzhou, 215123, P. R. China*

in the last few decades.[3–6] Despite remarkable progress in SSE-related studies (including the improvement of interfacial stability with electrode materials),[7–9] innovating electrode materials, particularly on the cathode side, remains a compelling strategy for enhancing the electrochemical performance of ASSLBs.

One of the purposes of developing cathode materials for ASSLBs is to realize high chemical compatibility with the SSEs, which have been extensively studied in recent years.[10–12] As shown in Fig. 1, since 2008, using sulfide-based SSEs, represented by Li argyrodites and $Li_{10}GeP_2S_{12}$-type (LGPS) materials,[13,14] high ionic conductivities up to 10^{-2} S cm^{-1} have been achieved.[9,15–17] While this achievement has mitigated the issue of sluggish ion transport in solids, sulfide SSEs are still suffering from severe interfacial challenges when paired with conventional layered oxide CAMs.[18,19] Additional interface modifications (*e.g.*, coatings) are necessary to improve the interface stability.[6,18,19] However, the reliance on coating methods and the presence of heterogeneous solid–solid interfaces increase system complexity and raise the barriers for practical applications.[20] Facing this dilemma, Tarascon and co-workers proposed sulfide cathode materials (*e.g.*, Li-rich $Li_{1.13}Ti_{0.57}Fe_{0.3}S_2$) to achieve good compatibility with sulfide superionic conductors.[21] The use of chemically homogeneous materials, such as sulfides for both electrolytes and cathodes, is beneficial for eliminating the space charge layer (SCL)[22] that arises from different chemical potentials between sulfides and oxides.[23]

As the latest generation of inorganic SSEs, halide-based SSEs have garnered increasing attention since Asano *et al.* reported Li_3YX_6 (X = Cl, Br)[3] in 2018, due to their favorable compatibility with conventional layered oxide cathodes.[25–28] In parallel, halide CAMs such as VX_3 (X = Cl, Br, I)[29] and $FeCl_3$,[30] which exhibit intrinsic thermodynamic stability with halide SSEs, have been revisited very recently for high-performance ASSLBs. During the same period, a variety of derivative compounds, including Li_3VCl_6,[31] $Li_{2.9}Fe_{0.9}Zr_{0.1}Cl_6$,[32] and Li_3TiCl_6,[33] were reported. These materials not only display redox activity but also feature a minimal difference between ionic and electronic conductivities (typically less than four orders of magnitude), enabling their application as either catholytes or CAMs.

Complementing these material innovations, Cui and co-workers proposed a breakthrough solution:[24] an interface-compatible dual-conductive (ICDC) sulfide-based cathode, specifically a Ge/Se co-doped $LiTi_2(PS_4)_3$ compound, can function independently as a cathode without the use of any conductive additives. This ICDC cathode can also be referred as a homogeneous cathode, which exhibits mixed ionic and electronic conductivity in a single material, avoids interfacial incompatibility-related reactions, and delivers a high specific capacity of 250 mA h g^{-1} with zero-strain behavior. Altogether, the development of high-performance ICDC cathodes represents

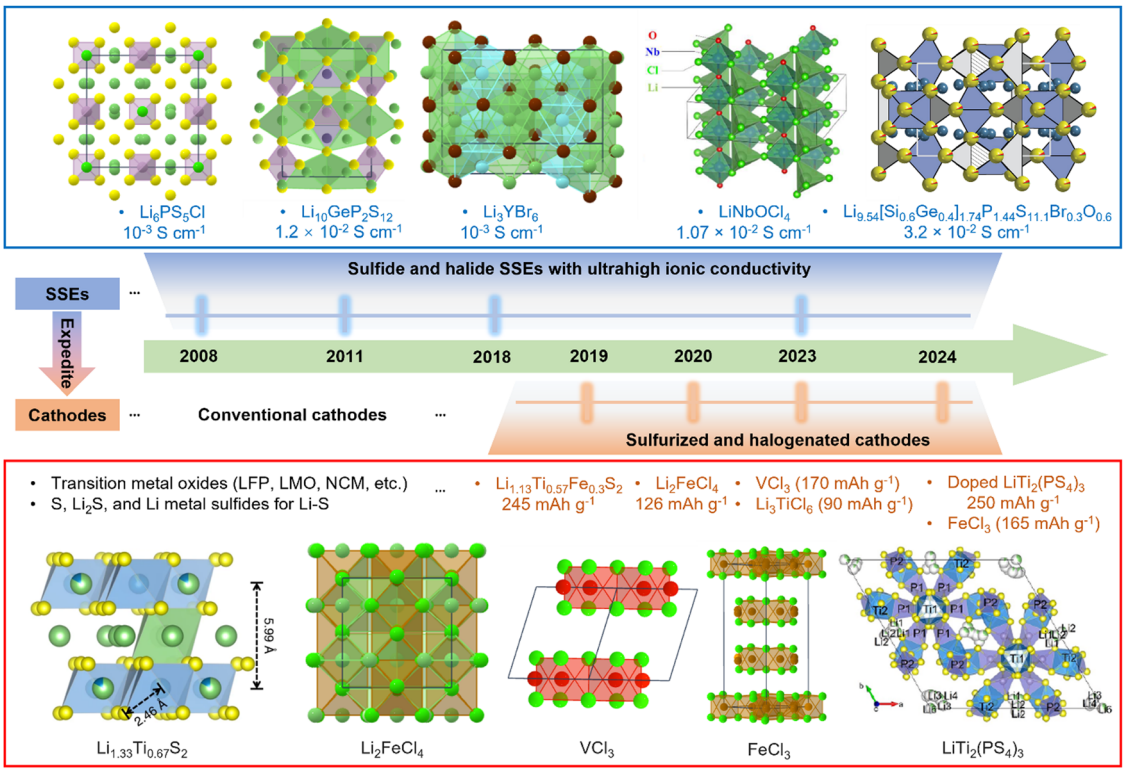

Fig. 1 Double timelines illustrating how the development of superionic conductors expedites the innovation of cathode materials. Schematic diagrams of the crystal structure are from the Materials Project database, except for $LiNbOCl_4$,[12] Copyright (2023), with permission from Wiley-VCH, LiSiGePSBrO (LGPS-type $Li_{9.54}[Si_{0.6}Ge_{0.4}]_{1.74}P_{1.44}S_{11.1}Br_{0.3}O_{0.6}$),[9] Copyright (2023), with permission from AAAS, $Li_{1.33}Ti_{0.67}S_2$,[21] Copyright (2019), with permission from Springer Nature, and $LiTi_2(PS_4)_3$.[24] Copyright (2024), with permission from Springer Nature.

a critical step toward realizing ASSLBs with high energy density, high power density, and extended cycle life.

Based on the above retrospect of mutual promotion between SSEs and cathode materials, we contend that the continuous advancement of SSEs is expediting the development of ICDC cathode materials specifically for ASSLBs. This emerging technical approach has been gradually gaining prominence, with ICDC cathodes demonstrating intrinsic compatibility with the state-of-the-art SSEs and exhibiting dual-conduction properties, thereby innovating the constitution of conventional cathode composites. In the following sections, we will elaborate on the necessity, experimental strategies, and characterization methods for developing ICDC cathode materials. In the end, we will propose several open questions about current ICDC cathodes and the extended research directions.

2. The necessity of developing ICDC cathodes

The issues of mismatched material chemistries and the need to form desirable cathode composites make the development of ICDC cathode materials necessary. As shown in Fig. 2, chemical potential discrepancies and inhomogeneous (de)lithiation are two major challenges when using conventional two/three-phase cathode composites. The former originates from mismatched chemistry among hetero-category materials. Taking the sulfide SSEs against conventional layered oxide CAMs as an example (Fig. 2a), oxides normally show a remarkably higher chemical potential than sulfides.[34] The resulting internal electric potential difference generates a SCL that reaches an equilibrium state.[22,35]

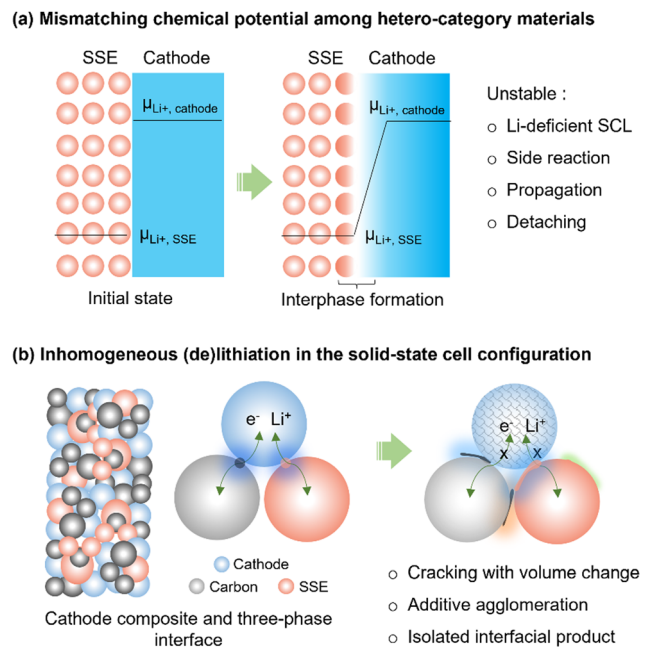

Fig. 2 Challenges in using conventional cathodes (*e.g.*, layered oxide cathodes) to pair up with the state-of-the-art SSEs (*e.g.*, sulfides and (oxy)-halides). (a) Mismatched materials lead to interface instability. (b) Inhomogeneity of materials impedes the ion/electron transport.

This layer is Li-deficient and hinders the ion transport across the oxide/sulfide interface, thereby limiting the utilization of CAMs. In addition, the mismatching of hetero-category materials leads to chemical side reactions. High-potential CAMs can oxidize elements such as sulfur and phosphorus in sulfide SSEs, while the metal elements in the CAMs are chemically reduced.[36] More critically, this uncontrollable interface can propagate, ultimately causing detachment between CAMs and SSEs, as well as between the cathode composite and the current collectors. Using ICDC cathodes that belong to the same material category as the involved SSEs is the most direct solution to solve the chemical potential discrepancy challenge. Therefore, for sulfide-based SSEs showing high ionic conductivity, it is necessary to develop sulfide cathode materials to establish a highly compatible cathode/SSE interface. In addition, halide-based SSEs share a similar chemical potential to those of oxides,[34] which significantly improves the compatibility compared to the sulfide/oxide interface. This helps explain the popularity of using halide SSEs as the catholytes for high-performance ASSLBs.[37]

The challenge of inhomogeneous (de)lithiation is attributed to the insufficient dual conduction in most conventional oxide CAMs. The ion and electron transport capabilities are essential for electrochemical reactions in batteries; yet conventional CAMs are not necessarily efficient ionic–electronic conductors (Table 1). As a result, additional ionic and/or electronic conducting additives are typically required in cathode composites to establish effective dual-conduction networks for ASSLBs. This introduces two/three-phase interfaces within the cathode composite (Fig. 2b). At these interfaces, volume changes associated with (de)intercalation in the CAMs and the decomposition of SSEs drive the agglomeration of ionic/electronic additives in certain regions while leaving others deficient. Such uneven distribution reduces the utilization of CAMs and causes continuous capacity fading. Meanwhile, the accompanied cracking of CAMs exposes fresh surfaces that may not be in contact with ionic/electronic additives, further deteriorating reversible capacity. Moreover, the presence of carbon additives exacerbates the degradation of SSEs (*e.g.*, sulfide SSEs) and promotes interfacial side reactions.[38,39] Consequently, avoiding or reducing carbon additives and SSEs in cathode composite fabrication has been gradually realized as important to mitigate the above negative effects.[40,41] In this context, developing ICDC cathode materials with satisfactory dual conductivity has become necessary. The concept of all-electrochemical-active (AEA) cathodes is the ultimate goal of ICDC cathodes.[42] The proposed materials feature superior mixed ionic–electronic mobility without any additional conductive additives. This approach enables a simplified cathode composition while maximizing the material usage efficiency.

3. General experimental routes toward ICDC cathode materials

3.1 Sulfurization

Sulfide-based SSEs, such as $Li_{10}GeP_2S_{12}$ and Li_6PSCl_5, exhibit electrochemical activity within specific voltage windows.[57,58]

Table 1 The dual conduction properties of the ICDC cathode materials compared with conventional CAMs

Cathode materials	Li-ion diffusion capability	Electronic conductivity (mS cm^{-1})	Voltage (V *vs.* Li/Li^+)	Specific capacity (mA h g^{-1})	Ref.
$Li_{1.75}Ti_2(Ge_{0.25}P_{0.75}S_{3.8}Se_{0.2})_3$	σ_{Li^+}: 0.22–0.66 mS cm^{-1}	242–412	2.55	250	24
$Li_{1.13}Ti_{0.57}Fe_{0.3}S_2$	—	20	2.5	214	21 and 43
O3–Li_xTiS_2	—	13.28	2.2–2.3	195	44
Li_3CuS_2	σ_{Li^+}: 3.3 × 10^{-3} mS cm^{-1}	9.5	2.1	380	45
Li_3NiS_4	—	2	2.25	400	46
Li_3VS_3	σ_{Li^+}: >0.1 mS cm^{-1}	>0.1	~2.1	437	47
$Li_{14}Mn_2S_9$	σ_{Li^+}: 0.011 mS cm^{-1}	—	~3.3	—	48
Cubic Li_2FeCl_4	σ_{Li^+}: 0.021 mS cm^{-1}; (D_{Li^+}: 2.8 × 10^{-10} cm^2 s^{-1})	—	3.6	126	49
Li_2FeCl_4 (*Cmmm* + *Imma*)	σ_{Li^+}: 0.01 mS cm^{-1}	2 × 10^{-4}	3.7	126	50
$FeCl_3$	—	—	3.65	159	30
Li_2VCl_4	σ_{Li^+}: 0.01–0.03 mS cm^{-1}	—	2.4	129.7	51
VCl_3	D_{Li^+}: 10^{-10} cm^2 s^{-1}	—	2.85	170	29
Li_3TiCl_6	1.04 mS cm^{-1}	7.3 × 10^{-4}	~3.2	~90	33
$LiCoO_2$	σ_{Li^+}: 10^{-4} mS cm^{-1} D_{Li^+}: 10^{-13}–10^{-11} cm^2 s^{-1}	0.1	3.9	140	52 and 53
$LiNi_{0.8}Co_{0.2}O_2$	σ_{Li^+}: 0.36–0.42 mS cm^{-1} D_{Li^+}: ~10^{-13} cm^2 s^{-1}	5.17	3.75	195	54
$LiNi_{0.8}Mn_{0.2}O_2$	σ_{Li^+}: 0.26–0.31 mS cm^{-1} D_{Li^+}: ~10^{-14} cm^2 s^{-1}	2.63	3.85	187	54
$LiFePO_4$	D_{Li^+}: 10^{-18}–10^{-14} cm^2 s^{-1}	10^{-6}	3.4	170	53 and 55
$LiMn_2O_4$	D_{Li^+}: 10^{-14}–10^{-11} cm^2 s^{-1}	10^{-3}	3.4	148	53 and 56

However, their poor reversibility, attributed to the covalent nature of metal–sulfur bonds, limits further development. A more practical strategy involves sulfurizing existing CAMs to achieve better interfacial stability and improve ionic/electronic conductivity. Notably, even a low degree of sulfurization has been shown to effectively enhance the compatibility between sulfide SSEs and conventional oxide CAMS, such as high-voltage $LiNi_{0.5}Mn_{1.5}O_4$ and high-nickel $LiNi_{0.88}Co_{0.09}Mn_{0.09}O_2$.[59,60] Additionally, fully sulfurized cathodes (sulfide cathodes) have been developed as an ideal category-matched solution for sulfide-based SSEs. Tarascon *et al.*[21] designed a Li-rich $Li_{1.13}Ti_{0.57}Fe_{0.3}S_2$ sulfide cathode material (Fig. 3a), showing a high electronic conductivity of 20 mS cm^{-1}. This value is higher than those of conventional oxide CAMs (Table 1). Fundamentally, replacing O with S in Li_2MnO_3 is impossible to obtain electrochemically active Li-rich sulfide cathode materials because the S 3p band is situated much closer to the Li/Li^+ reference than the O 2p band, leaving the $Mn^{3+/4+}$ redox band too low-lying. In contrast, Ti^{4+} is considered the most suitable 3d transition metal for creating sulfide cathodes, because the $Ti^{3+/4+}$ redox band is located above the S 3p band. However, Li_2TiS_3 is electrochemically inactive due to the $3d^0$ electronic configuration of Ti^{4+}. Therefore, metal doping (*e.g.*, Fe^{2+}, Co^{2+}, and Ti^{3+}) is necessary to activate redox activity. Due to the contribution from both cationic ($Fe^{2+/3+}$) and anionic (S^{2-}/S_n^-, $n < 2$) redox activity, a reversible capacity of ~245 mAh g^{-1} at an average voltage of ~2.5 V is realized for the $Li_{1.13}Ti_{0.57}Fe_{0.3}S_2$ material, achieving a specific energy of ~600 Wh kg^{-1}, which is comparable to that of $LiCoO_2$ (Fig. 3b).[21] However, the $Li_{1.13}Ti_{0.57}Fe_{0.3}S_2$ cathode material could not show a satisfactory capacity in a solid-state cell using β-Li_3PS_4 as the SSE, the reason could be ascribed to its insufficient ionic conductivity. It has actually been used as an electronic additive and integrated with $LiNi_{0.6}Mn_{0.2}Co_{0.2}O_2$ CAM to improve the cell performance.[43]

To enable dual conduction in one sulfide cathode material, multiple-element substitution associated with tuning the electronic structure of S has been carried out. For example, Cui *et al.*[24] employed Ge^{4+}/Se^{2-} co-doping into the structure of $LiTi_2(PS_4)_3$ to obtain an optimal composition of $Li_{1.75}Ti_2(Ge_{0.25}P_{0.75}S_{3.8}Se_{0.2})_3$ (abbreviated as $LTG_{0.25}PSSe_{0.2}$). This material shows Li^+/electronic conductivities of 0.22/242 mS cm^{-1} when fully charged, increasing monotonically to 0.66/412 mS cm^{-1} when fully discharged. As shown in Fig. 3c, the Se doping decreases the bandgap compared to using pure S, thus enhancing electronic conductivity. Ge incorporation reduces the number of delocalized electrons within the GeS_4 tetrahedra and facilitates the Li-ion migration. Due to the sufficient dual conduction, the $LTG_{0.25}PSSe_{0.2}$ sulfide cathode served as the only cathode layer without mixing with any carbon or SSEs to construct a high-performance ASSB, showing 70% capacity retention after 20 000 cycles at 2.5C. The extreme homogeneity of the lithiation process in $Li_{1.75}Ti_2(Ge_{0.25}P_{0.75}S_{3.8}Se_{0.2})_3$ was also illustrated by comparing to that of a conventional NCM811 cathode in the finite element analyses (Fig. 3d), and was believed to be the most important reason leading to the high performance. Based on the S-based cathode materials (*e.g.*, TiS_2 and Mo_9S_8) for ASSLBs, Li and Suo proposed a concept of using AEA materials as cathode.[42] As shown in Fig. 3e, a dense electrode is entirely constructed from AEA cathode, which can minimize the energy density gap between the accessible and theoretical energy density at the electrode level. AEA cathodes are a highly investigated family among the ICDC cathode materials, and have attracted increasing attention in constructing all-solid-state Li–S batteries (*e.g.*, Li_3VS_3,[47] Li_2TiS_3,[61] Li_3CuS_2,[45] Li_3NbS_4,[46] *etc.*). The main reason is due to the semi-conducing properties of transition metal sulfides, where the S^{2-}/S redox activity can be easily promoted even in the solid-state configuration.

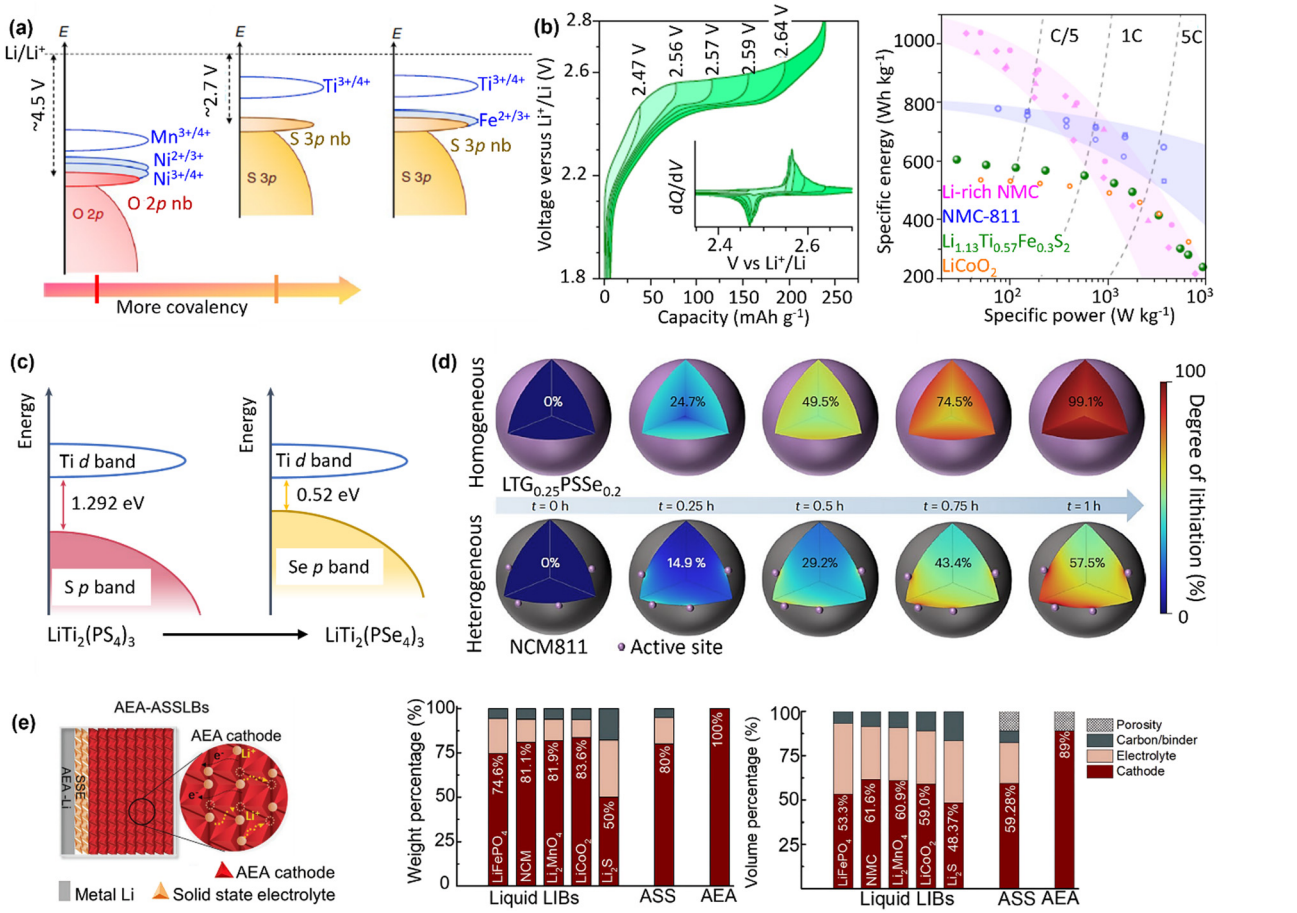

Fig. 3 Sulfurizing cathode materials. (a) Schematic band structure of Ni^{2+}-substituted $Li_{1.33}Mn_{0.67}O_2$ compared with $Li_{1.33}Ti_{0.67}S_2$ and its Fe^{2+}-substituted derivative. The label "nb" indicates non-bonding.[21] Copyright (2019), with permission from Springer Nature. (b) Voltage profiles of $Li_{1.13}Ti_{0.57}Fe_{0.3}S_2$ obtained from the charge-window opening experiment. Comparison of the Ragone plots of $Li_{1.13}Ti_{0.57}Fe_{0.3}S_2$ and typical cathode materials (NMC-811: $LiNi_{0.8}Mn_{0.1}Co_{0.1}O_2$).[21] Copyright (2019), with permission from Springer Nature. (c) Schematic band structure of $LiTi_2(PS_4)_3$ and $LiTi_2(PSe_4)_3$ guided by the density of states (DOS).[24] Copyright (2024), with permission from Springer Nature. (d) Finite element analysis simulating the lithiation behavior of one $LTG_{0.25}PSSe_{0.2}$ particle in the homogeneous cathode and one NCM811 particle in the heterogeneous cathode.[24] Copyright (2024), with permission from Springer Nature. (e) The scheme of an AEA-ASSLB (100 wt% AEA cathode, anode: Li metal) and the comparisons of the weight and volume percentages of various components in various battery configurations.[42] Copyright (2021), with permission from Wiley-VCH.

3.2 Halogenation

Halide cathode materials, achieved by a complete halogenation strategy, are naturally promising, considering the high theoretical capacity of metal halides and promising ionic conductivity of the discharged products (Li metal halides). However, the halides exhibit high solubility in liquid electrolytes, making them difficult to be used in the traditional LIBs.[62] This predicament has been changed since the revival of halide SSEs, as pairing halide cathodes with halide SSEs offers excellent chemical and structural homogeneity. As shown in Fig. 4a, the vanadium halide family VX_3 (X = Cl, Br, or I) have been reported as battery intercalation compounds that share a similar layered structure to that of cathode materials such as TiS_2 and $LiCoO_2$.[62] During the reversible charging and discharging, intermediate phases can be observed for VX_3 systems. However, the fully discharged phases differ depending on the nature of the anion (*e.g.*, the ionic radii $Cl^- < Br^- < I^-$). For VI_3, the fully discharged phase has a O1-type structure, while a O3-type layered structure was reported for those of VCl_3 and VBr_3.[62] On this theoretical basis, Liang *et al.* realized high-rate capability and stable operation of all-solid-state Li–VX_3 batteries (average voltage: ~2.9 V) by designing a compatible cathode interface between VCl_3 and Li_3InCl_6 SSEs.[29] As shown in Fig. 4b, the all-solid-state Li–VCl_3 battery exhibits a long cycle life of over 200 cycles with a capacity retention of 85% at a high rate of 6C. The redox potential of the transition metal determines the working voltage of halide cathode materials. While $V^{2+/3+}$ shows an intercalation voltage below 3 V, the $Fe^{2+/3+}$ redox in the chloride exhibits an unexpected voltage of ~3.65 V when integrating with $Li_{2.75}In_{0.75}Zr_{0.25}Cl_6$ as the catholyte in ASSLBs.[30] More importantly, the $FeCl_3$ cathode costs as little as 1% of the $LiCoO_2$ cathode or 2% of the $LiFePO_4$ cathode (Fig. 4c), while delivering a comparably high specific capacity of ~159 mA h g^{-1} and an energy density of ~558 Wh kg^{-1}.[30] The successful demonstration of using Li-deficient metal halide cathodes relies on using ionic and

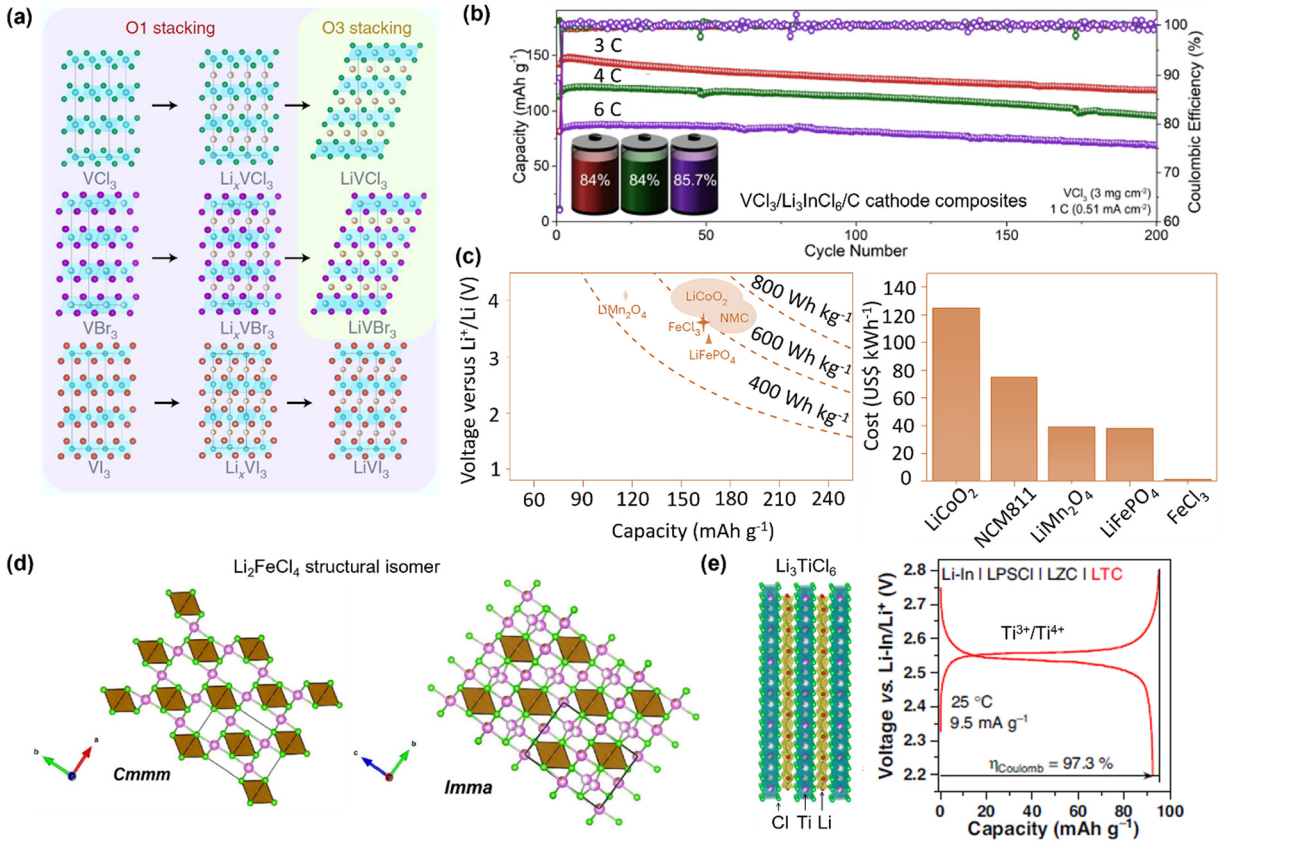

Fig. 4 Halogenating cathode materials. (a) Crystal structures of pristine, intermediate, and end-of-discharge phases for VCl_3, VBr_3 and VI_3 cathode materials.[62] Copyright (2021), with permission from Springer Nature. (b) Cycling stability of ASSLB using VCl_3–Li_3InCl_6–C cathode composites at 3, 4, and 6C. The battery schemes show the capacity retentions after 200 cycles.[29] Copyright (2023), with permission from Wiley-VCH. (c) Comparisons of voltage, specific capacity, and price between the $FeCl_3$ cathode and other various cathode materials.[30] Copyright (2024), with permission from Springer Nature. (d) Li_2FeCl_4 structures with *Cmmm* and *Imma* space groups.[50] Copyright (2024), with permission from ACS Publications. (e) A scheme of the layered crystal structure of Li_3TiCl_6, and the initial charge/discharge curve of the Li_3TiCl_6 cathode in a halide-based ASSLB that is based on the Ti^{3+}/Ti^{4+} redox.[33] Copyright (2023), with permission from Springer Nature.

electronic additives to achieve reversible (de)lithiation, thereby confirming the interfacial compatibility of homo-category materials, which are halide cathodes pairing halide SSEs. However, these studies overlooked detailed investigations of dual conductivity for the charged and discharged halide products.

Incorporating lithium into metal halides results in lithium metal halides with promising ionic conductivity, while partially retaining the electronic conductivity influenced by the electronic structure of the transition metal. The cubic-type Li_2FeCl_4 that was previously only regarded as an ionic conductor (2.1×10^{-5} S cm^{-1}) has been first revealed to show a redox activity (126 mA h g^{-1}/3.6 V).[49] Similarly, Li_2VCl_4 with an ionic conductivity of 1–3 $\times$ 10^{-5} S cm^{-1} was reported to show a reversible specific capacity of 129.7 mA h g^{-1} in ASSLBs, when mixed with 10 wt% of carbon to prepare a cathode composite.[51] The Li_2FeCl_4 cathode prepared by ball-milling and post-annealing crystallizes in a $SnMn_2S_4$-type NaCl superstructure (*Cmmm*) with a small portion of the ordered spinel superstructure (*Immm*) (Fig. 4d).[50] This Li_2FeCl_4 features Li^+/electronic conductivities of $0.01/2 \times 10^{-4}$ mS cm^{-1}, respectively. When tested in ASSLBs, the material shows a highly reversible Li (de)intercalation at 3.7 V, and good cycling stability with an 86% capacity retention after 6000 cycles at 2C. A dual-conductive Li_3TiCl_6 with Li^+/electronic conductivities of $1.04/(7 \times 10^{-4})$ mS cm^{-1} can serve as electrode material based on the $Ti^{3+/4+}$ and Ti^{2+}/Ti^{3+}redox couples, delivering a reversible capacity of ~90 mA h g^{-1} (Fig. 4e).[33] It is worth noting that the Li_3TiCl_6 CAM in the Li_3TiCl_6/C cathode composite can comprise up to 95 wt%, which is significantly higher than the typical loading (<80 wt%) for layered oxide cathodes. Compared to the sulfurization approach, the dual conduction properties achieved *via* halogenation have not reached a similarly high level. However, the halogenation route has been gradually leading to the innovative development of homogenous cathode materials for ASSLBs because halides show relatively high working potential and capacity that is comparable with several typical oxide cathode materials.

4. Characterization of ICDC cathode materials

One of the challenges with ICDC materials is the dynamic changes of their structure and dual conductivity during charging/discharging processes. To reveal the dynamic evolution,

in situ/*operando* neutron/X-ray scattering and spectroscopy techniques, such as pair distribution function (PDF), X-ray diffraction (XRD), and solid-state nuclear magnetic resonance (ss-NMR), can be coupled with electrochemical techniques to analyze the structures as well as the migration and conduction of Li ions.[63]

Electrochemo-mechanical failures would be another challenge related to ICDC cathodes. Imaging techniques, such as X-ray computed tomography (XCT), can reflect the morphology changes within a cold/hot-pressed pellet without destructing the material. Electrochemical techniques combined with pressure/stress monitoring are also non-destructive and effective tools,[64] which can qualitatively reflect the reaction kinetics and volume changes within ICDC cathodes and SSE particles. For understanding electrochemo mechanisms in detail, spectroscopy techniques (Raman, mass spectroscopy, X-ray absorption spectroscopy (XAS), *etc*) can be used to reveal the *in situ* generated interphases by providing information regarding the structure of molecules, the oxidation state of the interested elements, and the local chemical environment. Nowadays, artificial intelligence techniques (such as deep learning) are popular, and are coupled with advanced imaging techniques to identity the unknown phases.[65] Designing home-made *in situ*/*operando* set ups and coupling two or more techniques (such as XCT-pressure monitoring[66]) together seem to be more powerful to get comprehensive information about the ICDC cathode materials.[67]

5. Summary and outlook

With the rapid advancements in SSEs leading to significantly improved ionic conductivity, ICDC cathode materials—developed through sulfurization and halogenation routes—have recently been introduced to address cathode interface challenges posed by advanced SSEs. Designing high performance ICDC cathodes requires two fundamental principles. As shown in Fig. 5, the first is ensuring a homo-category alignment with the SSEs used in the solid-state configuration, minimizing the chemical potential gap to prevent interfacial mismatches. The second one is achieving dual conduction of Li ions and electrons within a single CAM, enabling a higher proportion of the CAM in the cathode composite or even in the AEA configuration, and eliminating inhomogeneous (de)lithiation.

Despite significant progresses, research on ICDC cathodes remains in its early stage, with several open questions and underexplored fields requiring further investigation:

(1) Dynamic evolution and dual conduction: current ICDC cathodes exhibit dual-conduction properties (Li ions and electrons), but their structures and morphologies evolve dynamically during charging/discharging. The intermediate charged/discharged products may show variations in the conduction properties, which are still poorly understood. Moreover, to enable a better comparison with conventional cathodes and SSEs, a standard protocol for describing ion transport capability of ICDC cathodes in ASSLBs, using either the Li-ion diffusion coefficient or Li-ion conductivity, should be established.

(2) Cathode–cathode and cathode–electrolyte interfaces: first, the intrinsic "solid-solid" contact is poor, resulting in pores, voids and grain boundaries among ICDC cathode and SSE particles. Second, the *in situ* formed cathode–cathode and cathode–electrolyte interfaces, such as interphases, gas, and/or contact loss, can directly affect the performance of ASSLBs. Amorphous thin films and self-healing crystals with good ductility and zero strain are promising for addressing these issues.

(3) Insufficient working potential: the working potential of current homogeneous cathode materials remains low, with a maximum of 3.7 V achieved by the $Fe^{2+/3+}$ redox in halide-based cathodes. While $FeCl_3$-based cathodes deliver energy densities comparable to $LiCoO_2$, they fall short compared to Ni-rich layered oxide cathodes and other high-voltage cathodes. To bridge this

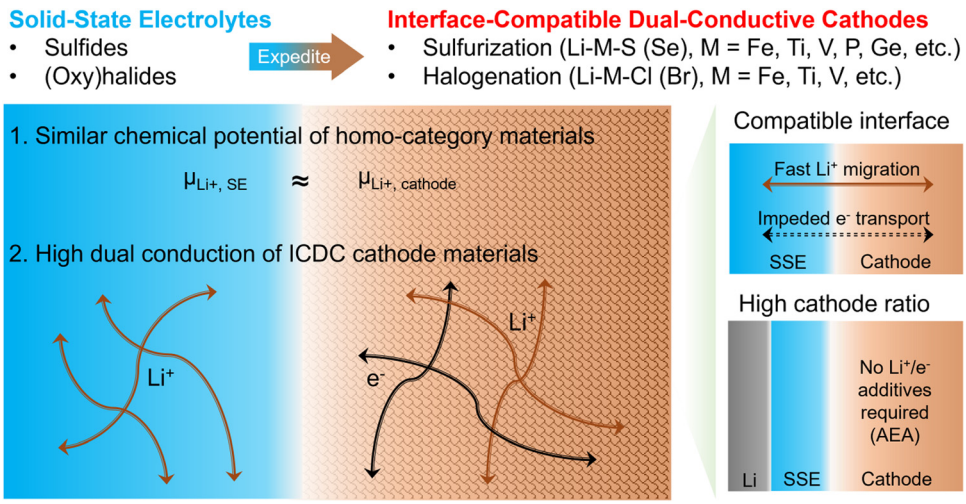

Fig. 5 Illustrative diagram depicting the design principle for developing homogenous cathode materials for ASSLBs based on advanced sulfide or (oxy)chloride SSEs.

gap, future research should focus on designing high-voltage ICDC cathodes, considering the electronegativity of the elements and the selection of counterions to enhance electrochemical potential. Modifying the existing materials would be another route for achieving desirable electrochemical potential of ICDC cathodes. Their crystallinity, inner defects, and particle size can affect the site energy of ions and the band energy state of electrons, which determines the voltage profiles of the targeted materials. However, achieving high-voltage ICDC cathodes with satisfactory dual conductivity remains a major challenge, especially for developing ICDC cathodes containing electronegative anions while maintaining decent ionic conductivity simultaneously.

(4) Expanding ICDC properties to anodes: in fact, a Li metal anode can be treated approximately as an AEA material, in which both Li ions and electrons can effectively diffuse at the Li–SSE interface. However, interfacial instability between the Li metal and SSEs is severe, mainly resulting from the reduction of SSEs and dendrite growth. Extending the concept of ICDC electrode materials to anodes may improve the interfacial compatibility at the anode side, for example, modifying the existing dendrite-free $Li_4Ti_5O_{12}$-based systems. While non-Li metal anodes show higher working potentials and the use of them would sacrifice energy density, their ability to enhance long-term stability and suppress dendrite formation presents a promising pathway for practical development of ASSLBs.

(5) Extension beyond lithium systems: the ICDC strategy can be extended to other solid-state systems, such as all-solid-state sodium batteries, for both cathode and anode applications. For Na-based chemistry, the development of homogeneous approaches beyond sulfurization and halogenation is needed. For instance, new materials compatible with Na-based superionic conductors (*e.g.*, borohydride SSEs) could be explored. Demonstrating the universality of the ICDC strategy in different systems would further validate its potential and accelerate the development of high-energy-density and safe solid-state batteries.

Data availability

No primary research results, software or code have been included and no new data were generated or analysed as part of this review.

Conflicts of interest

There are no conflicts to declare.

Acknowledgements

S. Z. acknowledges the research start-up funding from Soochow University. L. L. acknowledges the support from the National Natural Science Foundation of China (52025028, 52332008). X. S. acknowledges the support from the National Natural Science Foundation of China (W2441017).

References

1 J. Janek and W. G. Zeier, *Nat. Energy*, 2023, **8**, 230–240.
2 Y. S. Meng, V. Srinivasan and K. Xu, *Science*, 2022, **378**, eabq3750.
3 T. Asano, A. Sakai, S. Ouchi, M. Sakaida, A. Miyazaki and S. Hasegawa, *Adv. Mater.*, 2018, **30**, 1803075.
4 Y.-C. Yin, J.-T. Yang, J.-D. Luo, G.-X. Lu, Z. Huang, J.-P. Wang, P. Li, F. Li, Y.-C. Wu, T. Tian, Y.-F. Meng, H.-S. Mo, Y.-H. Song, J.-N. Yang, L.-Z. Feng, T. Ma, W. Wen, K. Gong, L.-J. Wang, H.-X. Ju, Y. Xiao, Z. Li, X. Tao and H.-B. Yao, *Nature*, 2023, **616**, 77–83.
5 W. Xia, Y. Zhao, F. P. Zhao, K. G. Adair, R. Zhao, S. Li, R. Q. Zou, Y. S. Zhao and X. L. Sun, *Chem. Rev.*, 2022, **122**, 3763–3819.
6 D. H. S. Tan, Y. S. Meng and J. Jang, *Joule*, 2022, **6**, 1755–1769.
7 H. L. Wan, J. J. Xu and C. S. Wang, *Nat. Rev. Chem.*, 2024, **8**, 30–44.
8 G. P. Han, A. Vasylenko, L. M. Daniels, C. M. Collins, L. Corti, R. Y. Chen, H. J. Niu, T. D. Manning, D. Antypov, M. S. Dyer, J. Lim, M. Zanella, M. Sonni, M. Bahri, H. Jo, Y. Dang, C. M. Robertson, F. Blanc, L. J. Hardwick, N. D. Browning, J. B. Claridge and M. J. Rosseinsky, *Science*, 2024, **383**, 739–745.
9 Y. Li, S. Song, H. Kim, K. Nomoto, H. Kim, X. Sun, S. Hori, K. Suzuki, N. Matsui, M. Hirayama, T. Mizoguchi, T. Saito, T. Kamiyama and R. Kanno, *Science*, 2023, **381**, 50–53.
10 H. Kwak, S. Wang, J. Park, Y. S. Liu, K. T. Kim, Y. Choi, Y. F. Mo and Y. S. Jung, *ACS Energy Lett.*, 2022, **7**, 1776–1805.
11 X. Y. Feng, H. Fang, N. Wu, P. C. Liu, P. Jena, J. Nanda and D. Mitlin, *Joule*, 2022, **6**, 543–587.
12 Y. Tanaka, K. Ueno, K. Mizuno, K. Takeuchi, T. Asano and A. Sakai, *Angew. Chem., Int. Ed.*, 2023, **62**, e202217581.
13 H. J. Deiseroth, S. T. Kong, H. Eckert, J. Vannahme, C. Reiner, T. Zaiss and M. Schlosser, *Angew. Chem., Int. Ed.*, 2008, **47**, 755–758.
14 N. Kamaya, K. Homma, Y. Yamakawa, M. Hirayama, R. Kanno, M. Yonemura, T. Kamiyama, Y. Kato, S. Hama, K. Kawamoto and A. Mitsui, *Nat. Mater.*, 2011, **10**, 682–686.
15 P. Adeli, J. D. Bazak, K. H. Park, I. Kochetkov, A. Huq, G. R. Goward and L. F. Nazar, *Angew. Chem., Int. Ed.*, 2019, **58**, 8681–8686.
16 L. D. Zhou, A. Assoud, Q. Zhang, X. H. Wu and L. F. Nazar, *J. Am. Chem. Soc.*, 2019, **141**, 19002–19013.
17 Y. Kato, S. Hori, T. Saito, K. Suzuki, M. Hirayama, A. Mitsui, M. Yonemura, H. Iba and R. Kanno, *Nat. Energy*, 2016, **1**, 16030.
18 Q. Zhang, D. Cao, Y. Ma, A. Natan, P. Aurora and H. Zhu, *Adv. Mater.*, 2019, **31**, 1901131.
19 C. H. Wang, J. W. Liang, Y. Zhao, M. T. Zheng, X. N. Li and X. L. Sun, *Energy Environ. Sci.*, 2021, **14**, 2577–2619.
20 S. P. Culver, R. Koerver, W. G. Zeier and J. Janek, *Adv. Energy Mater.*, 2019, **9**, 1900626.
21 S. Saha, G. Assat, M. T. Sougrati, D. Foix, H. Li, J. Vergnet, S. Turi, Y. Ha, W. Yang, J. Cabana, G. Rousse, A. M. Abakumov and J.-M. Tarascon, *Nat. Energy*, 2019, **4**, 977–987.

22 J. Haruyama, K. Sodeyama, L. Y. Han, K. Takada and Y. Tateyama, *Chem. Mater.*, 2014, **26**, 4248–4255.
23 L. Wang, R. Xie, B. Chen, X. Yu, J. Ma, C. Li, Z. Hu, X. Sun, C. Xu, S. Dong, T. S. Chan, J. Luo, G. Cui and L. Chen, *Nat. Commun.*, 2020, **11**, 5889.
24 L. Cui, S. Zhang, J. Ju, T. Liu, Y. Zheng, J. Xu, Y. Wang, J. Li, J. Zhao, J. Ma, J. Wang, G. Xu, T.-S. Chan, Y.-C. Huang, S.-C. Haw, J.-M. Chen, Z. Hu and G. Cui, *Nat. Energy*, 2024, **9**, 1084–1094.
25 S. Zhang, F. Zhao, J. Chen, J. Fu, J. Luo, S. H. Alahakoon, L.-Y. Chang, R. Feng, M. Shakouri, J. Liang, Y. Zhao, X. Li, L. He, Y. Huang, T.-K. Sham and X. Sun, *Nat. Commun.*, 2023, **14**, 3780.
26 C. Wang, J. Liang, J. T. Kim and X. Sun, *Sci. Adv.*, 2022, **8**, eadc9516.
27 S. Yu, J. Noh, B. Kim, J.-H. Song, K. Oh, J. Yoo, S. Lee, S.-O. Park, W. Kim, B. Kang, D. Kil and K. Kang, *Science*, 2023, **382**, 573–579.
28 F. P. Zhao, S. M. Zhang, S. Wang, C. M. Andrei, H. Yuan, J. G. Zhou, J. Wang, Z. Q. Zhuo, Y. Zhong, H. Su, J. T. Kim, R. Z. Yu, Y. J. Gao, J. H. Guo, T. K. Sham, Y. F. Mo and X. L. Sun, *Energy Environ. Sci.*, 2024, **17**, 4055–4063.
29 J. W. Liang, X. N. Li, J. T. Kim, X. G. Hao, H. Duan, R. Y. Li and X. L. Sun, *Angew. Chem., Int. Ed.*, 2023, **135**, e202217081.
30 Z. Liu, J. Liu, S. Zhao, S. Xun, P. Byaruhanga, S. Chen, Y. Tang, T. Zhu and H. Chen, *Nat. Sustainability*, 2024, **7**, 1492–1500.
31 Z. Y. Song, Y. M. Dai, T. R. Wang, Q. Yu, X. L. Ye, L. K. Wang, Y. N. Zhang, S. T. X. Wang and W. Luo, *Adv. Mater.*, 2024, **36**, 2405277.
32 G. X. Zhang, Z. T. Liu, Y. F. Ma, J. Pepas, J. M. Bai, H. Zhong, Y. Z. Tang and H. L. Chen, *Chem. Mater.*, 2024, **36**, 10104–10112.
33 K. Wang, Z. Gu, Z. Xi, L. Hu and C. Ma, *Nat. Commun.*, 2023, **14**, 1396.
34 S. Wang, Q. Bai, A. M. Nolan, Y. S. Liu, S. Gong, Q. Sun and Y. F. Mo, *Angew. Chem., Int. Ed.*, 2019, **58**, 8039–8043.
35 K. Takada, N. Ohta, L. Q. Zhang, K. Fukuda, I. Sakaguchi, R. Ma, M. Osada and T. Sasaki, *Solid State Ionics*, 2008, **179**, 1333–1337.
36 F. Zhao, S. Zhang, Y. Li and X. Sun, *Small Struct.*, 2022, **3**, 2100146.
37 J. K. Eckhardt, S. Kremer, L. Merola and J. Janek, *ACS Appl. Mater. Interfaces*, 2024, **16**, 18222–18235.
38 H. S. Kim, S. Park, S. R. Kang, J. Y. Jung, K. Kim, J. S. Yu, D. W. Kim, J. W. Lee, Y. K. Sun and W. S. Cho, *Adv. Funct. Mater.*, 2024, **34**, 2409318.
39 K. Yoon, J. J. Kim, W. M. Seong, M. H. Lee and K. Kang, *Sci. Rep.*, 2018, **8**, 8066.
40 L. S. Li, H. H. Duan, J. Li, L. Zhang, Y. F. Deng and G. H. Chen, *Adv. Energy Mater.*, 2021, **11**, 2003154.
41 S. Puls, E. Nazmutdinova, F. Kalyk, H. M. Woolley, J. F. Thomsen, Z. Cheng, A. Fauchier-Magnan, A. Gautam, M. Gockeln, S. Y. Ham, M. T. Hasan, M. G. Jeong, D. Hiraoka, J. S. Kim, T. Kutsch, B. Lelotte, P. Minnmann, V. Miss, K. Motohashi, D. L. Nelson, F. Ooms, F. Piccolo, C. Plank, M. Rosner, S. E. Sandoval, E. Schlautmann, R. Schuster, D. Spencer-Jolly, Y. P. Sun, B. S. Vishnugopi, R. Z. Zhang, H. Zheng, P. Adelhelm, T. Brezesinski, P. G. Bruce, M. Danzer, M. El Kazzi, H. Gasteiger, K. B. Hatzell, A. Hayashi, F. Hippauf, J. Janek, Y. S. Jung, M. T. McDowell, Y. S. Meng, P. P. Mukherjee, S. Ohno, B. Roling, A. Sakuda, J. Schwenzel, X. L. Sun, C. Villevieille, M. Wagemaker, W. G. Zeier and N. M. Vargas-Barbosa, *Nat. Energy*, 2024, **9**, 1310–1320.
42 M. Y. Li, T. Liu, Z. Shi, W. J. Xue, Y. S. Hu, H. Li, X. J. Huang, J. Li, L. M. Suo and L. Q. Chen, *Adv. Mater.*, 2021, **33**, 2008723.
43 F. Marchini, S. Saha, D. Alves Dalla Corte and J. M. Tarascon, *ACS Appl. Mater. Interfaces*, 2020, **12**, 15145–15154.
44 B. Hennequart, M. Deschamps, R. Chometon, B. Leube, R. Dugas, E. Quemin, P.-E. Cabelguen, C. Lethien and J.-M. Tarascon, *ACS Appl. Energy Mater.*, 2023, **6**, 8521–8531.
45 Y. Kawasaki, H. Tsukasaki, T. Ayama, S. Mori, M. Deguchi, M. Tatsumisago, A. Sakuda and A. Hayashi, *ACS Appl. Energy Mater.*, 2021, **4**, 20–24.
46 A. Sakuda, T. Takeuchi, M. Shikano, H. Sakaebe and H. Kobayashi, *Front. Energy Res.*, 2016, **4**, 19.
47 T. Shigedomi, Y. Fujita, T. Kishi, K. Motohashi, H. Tsukasaki, H. Nakajima, S. Mori, M. Tatsumisago, A. Sakuda and A. Hayashi, *Chem. Mater.*, 2022, **34**, 9745–9752.
48 J. F. Yang Qifan; X. Xiao; L. Jingchen; W. Liqi; G. Xuhe; W. Zibin; X. Ruijuan and L. Hong, 2024, arXiv:2410.15350.
49 N. Tanibata, M. Kato, S. Takimoto, H. Takeda, M. Nakayama and H. Sumi, *Adv. Energy Sustainability Res.*, 2020, **1**, 2000025.
50 Z. Liu, G. Zhang, J. Pepas, Y. Ma and H. Chen, *ACS Energy Lett.*, 2024, **9**, 5464–5470.
51 T. Kasahara, P. Song, I. Honma and S. Ohno, *Batteries Supercaps*, 2024, **8**, e202400520.
52 H. Xia, L. Lu and G. Ceder, *J. Power Sources*, 2006, **159**, 1422–1427.
53 G. Kucinskis, G. Bajars and J. Kleperis, *J. Power Sources*, 2013, **240**, 66–79.
54 S. Lee, D. Lee and A. Manthiram, *J. Mater. Chem. A*, 2024, **12**, 26244–26252.
55 C. S. Wang and J. Hong, *Electrochem. Solid-State Lett.*, 2007, **10**, A65–A69.
56 N. Kuwata, M. Nakane, T. Miyazaki, K. Mitsuishi and J. Kawamura, *Solid State Ionics*, 2018, **320**, 266–271.
57 T. K. Schwietert, V. A. Arszelewska, C. Wang, C. Yu, A. Vasileiadis, N. J. J. de Klerk, J. Hageman, T. Hupfer, I. Kerkamm, Y. L. Xu, E. van der Maas, E. M. Kelder, S. Ganapathy and M. Wagemaker, *Nat. Mater.*, 2020, **19**, 428–435.
58 F. Han, T. Gao, Y. Zhu, K. J. Gaskell and C. Wang, *Adv. Mater.*, 2015, **27**, 3473–3483.
59 Y. Wang, Y. Lv, Y. Su, L. Chen, H. Li and F. Wu, *Nano Energy*, 2021, **90**, 106589.
60 Y. Wang, Z. Wang, D. Wu, Q. Niu, P. Lu, T. Ma, Y. Su, L. Chen, H. Li and F. Wu, *eScience*, 2022, **2**, 537–545.
61 Y. Hu, Z. Sun, Z. Zhang, S. Liu, F. He, Y. Liu, Z. Zhuang and F. Liu, *Adv. Energy Mater.*, 2022, **13**, 2202756.

62 N. Dubouis, T. Marchandier, G. Rousse, F. Marchini, F. Fauth, M. Avdeev, A. Iadecola, B. Porcheron, M. Deschamps, J. M. Tarascon and A. Grimaud, *Nat. Mater.*, 2021, **20**, 1545–1550.
63 E. P. Alsaç, D. L. Nelson, S. G. Yoon, K. A. Cavallaro, C. C. Wang, S. E. Sandoval, U. D. Eze, W. J. Jeong and M. T. Mcdowell, *Chem. Rev.*, 2025, **125**, 2009–2119.
64 X. Li, J. Liang, J. T. Kim, J. Fu, H. Duan, N. Chen, R. Li, S. Zhao, J. Wang, H. Huang and X. Sun, *Adv. Mater.*, 2022, **34**, e2200856.
65 M. Kodama, A. Ohashi, H. Adachi, T. Miyuki, A. Takeuchi, M. Yasutake, K. Uesugi, T. Kaburagi and S. Hirai, *J. Power Sources Adv.*, 2021, **8**, 100048.
66 Y. Sakka, H. Yamashige, A. Watanabe, A. Takeuchi, M. Uesugi, K. Uesugi and Y. Orikasa, *J. Mater. Chem. A*, 2022, **10**, 16602–16609.
67 S. M. Bak, Z. Shadike, R. Q. Lin, X. Q. Yu and X. Q. Yang, *NPG Asia Mater.*, 2018, **10**, 563–580.